Draft version August 7, 2013
Preprint typeset using LaTeX style emulateapj v. 5/2/11

THE DUST ATTENUATION LAW IN DISTANT GALAXIES: EVIDENCE FOR VARIATION WITH SPECTRAL TYPE

Mariska Kriek[1], & Charlie Conroy[2]

Draft version August 7, 2013

ABSTRACT

This letter utilizes composite spectral energy distributions (SEDs) constructed from NEWFIRM Medium-Band Survey photometry to constrain the dust attenuation curve in $0.5 < z < 2.0$ galaxies. Based on similarities between the full SED shapes (0.3-8μm), we have divided galaxies in 32 different spectral classes and stacked their photometry. As each class contains galaxies over a range in redshift, the resulting rest-frame SEDs are well-sampled in wavelength and show various spectral features including Hα and the UV dust bump at 2175 Å. We fit all composite SEDs with flexible stellar population synthesis models, while exploring attenuation curves with varying slopes and UV bump strengths. The Milky Way and Calzetti law provide poor fits at UV wavelengths for nearly all SEDs. We find a strong correlation between the best-fit slope and the bump strength, with steeper laws having stronger UV bumps. Moreover, the attenuation curve correlates with the specific star formation rate (SFR), such that galaxies with higher specific SFRs have shallower dust curves with weaker UV bumps. There is also a weak correlation with inclination, which may be suggestive of a two-component dust model. A varying grain size distribution, as a result of differences in UV radiation fields may also contribute to the observed trends. Our results have several implications for galaxy evolution studies. First, the assumption of a universal dust model will lead to biases in derived galaxy properties. Second, the presence of a dust bump may result in underestimated values for the UV slope, used to correct SFRs of distant galaxies.

Subject headings: dust, extinction — galaxies: stellar content

1. INTRODUCTION

After dark matter, dust may be the most mysterious component of galaxies. Aside from the Milky Way (MW) and a few well-studied galaxies, we know little about the types of grains, the distribution of dust with respect to stars, the dust to gas or dust to star ratio, or the dust production and destruction cycle. Consequently, the role of dust within the baryon cycle of galaxies is poorly understood. We know that dust affects the energy balance in the interstellar medium (ISM), the cooling of gas, and hence star formation. However, dust is currently not included in theoretical galaxy evolution models, and appropriate observations needed to constrain these processes are still missing. Moreover, in order to study the stellar populations of galaxies, we must have a solid understanding of the properties and spatial distribution of dust.

When deriving the properties of distant galaxies from photometric or spectroscopic observations, we commonly assume a uniform attenuation law, often implemented as a simple screen. Yet we know that the dust attenuation law is not universal. For example, the MW and the Large Magellanic Cloud (LMC) extinction curve to a lesser extent exhibit a dust absorption feature around 2175 Å (Stecher 1965), which is absent in 4 out of 5 sight-lines toward the Small Magellanic Cloud (SMC) and in an empirical attenuation curve for starburst galaxies (Calzetti et al. 2000). This feature has been seen in other galaxies as well, out to $z \sim 1$ or even higher, though not as strong as for the Milky Way (e.g., Burgarella et al. 2005; Noll et al. 2009; Elíasdottír et al. 2009; Conroy et al. 2010b; Conroy 2010; Wild et al. 2011; Buat et al. 2011). The slope of the attenuation curve also varies among different sight-lines and galaxies.

Variations in the dust attenuation curve are expected on theoretical grounds (Witt & Gordon 2000). However, the origin of the observed differences between the various laws are poorly understood. For example, we do not know what types of grains are responsible for the 2175 Å dust bump (e.g., Draine & Malhotra 1993), nor what physical process governs its strength. We stress that dust attenuation and extinction are distinct concepts; attenuation includes dust geometry and radiative transfer effects, which may in part explain the observed differences.

In order to understand the role of dust and to correct the integrated light from galaxies, we need to gain a better understanding of the processes shaping the dust attenuation curve. The dust attenuation curve can be derived from the stellar light of galaxies, but it requires wide wavelength coverage and sufficient spectral resolution. Both requirements are needed to break degeneracies with other modeling parameters, such as stellar age and star formation timescale (e.g., Labbé et al. 2005) and to directly detect the UV dust bump. This combination has recently become feasible with the completion of the NEWFIRM Medium-Band Survey (NMBS; Whitaker et al. 2011; van Dokkum et al. 2009). In this Letter we use well-sampled composite SEDs constructed from the NMBS photometry (Kriek et al. 2011), in combination with the flexible SPS models (FSFS; Conroy et al. 2009, 2010a; Conroy & Gunn 2010), to

[1] Astronomy Department, University of California at Berkeley, Berkeley, CA 94720
[2] Department of Astronomy & Astrophysics, University of California at Santa Cruz, Santa Cruz, CA 95064

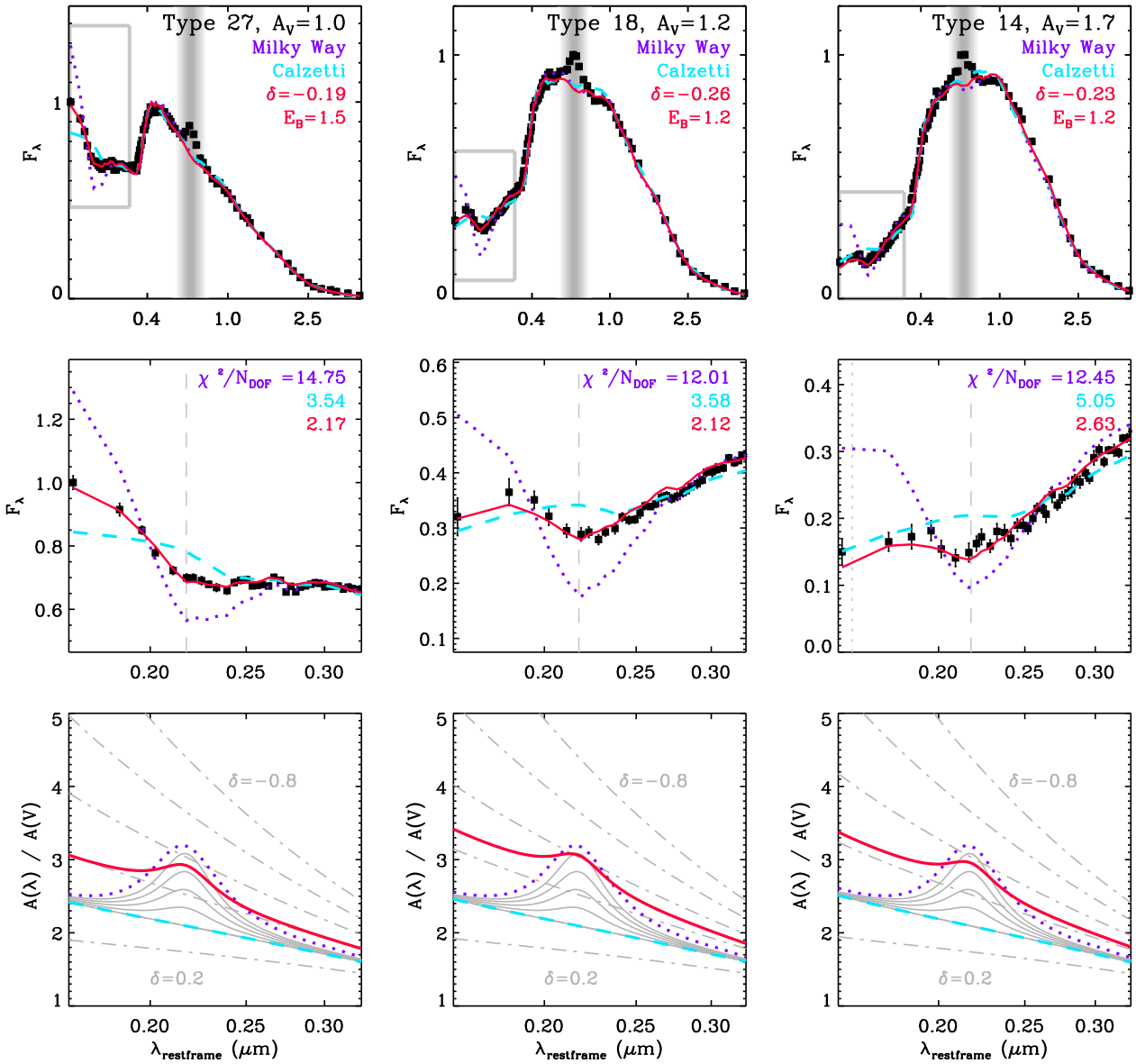

Figure 1. Composite SEDs for three arbitrarily chosen galaxy types, ordered by increasing value of A_V. The top panels show the full wavelength range and the middle panels zoom in on the gray open box in the rest-frame UV. The gray shaded area indicates the region around Hα. The best-fit SPS models for different dust attenuation curves are overplotted. We explore the Calzetti law (light blue), the MW law (purple), and a dust law in which the slope (δ) and strength of the UV bump (E_b) are free parameters (red). The corresponding attenuation curves are shown in the bottom panel. The explored range in values for the slope ($\delta = [-0.8, 0.2]$) and UV bump strength ($E_b = [0, 4]$) are represented by the dashed-dotted and solid gray curves in the bottom panels. Both the Calzetti and the MW dust law provide poor fits in the rest-frame UV.

constrain the dust attenuation curve in $0.5 < z < 2.0$ galaxies.

2. DATA

The NMBS is a 0.5 square degree photometric survey in the COSMOS and AEGIS fields, unique for its 5 customly designed medium-band near-infrared filters. The photometry of these filters is combined with optical-to-MIR photometry. For this study we make use of the NMBS catalogs in the COSMOS field, which include medium-band photometry at optical wavelengths as well. When no spectroscopic redshifts are available, we use photometric redshifts (EAzY; Brammer et al. 2008), which have an accuracy of $\Delta z/(1+z) < 0.02$ (Whitaker et al. 2011; Kriek et al. 2011; Brammer et al. 2011). The high quality of the NMBS photometry has been illustrated in van Dokkum et al. (2010) and Whitaker et al. (2010, 2012).

In Kriek et al. (2011) we divided all NMBS galaxies at $0.5 < z < 2.0$ and with a $S/N_K > 25$ into different spectral classes, based on their observed optical-to-IRAC SEDs. Each spectral class contains 22-455 individual galaxies of similar spectral shape. For each class we constructed a composite SED, by de-redshifting and scaling the observed photometry. These composite SEDs are basically low-resolution spectra ($R \lesssim 25$, Fig. 1), and show many spectral features among which Hα which is blended with [N II] and [S II] and the blended [O III] and Hβ lines. Continuum and absorption features are

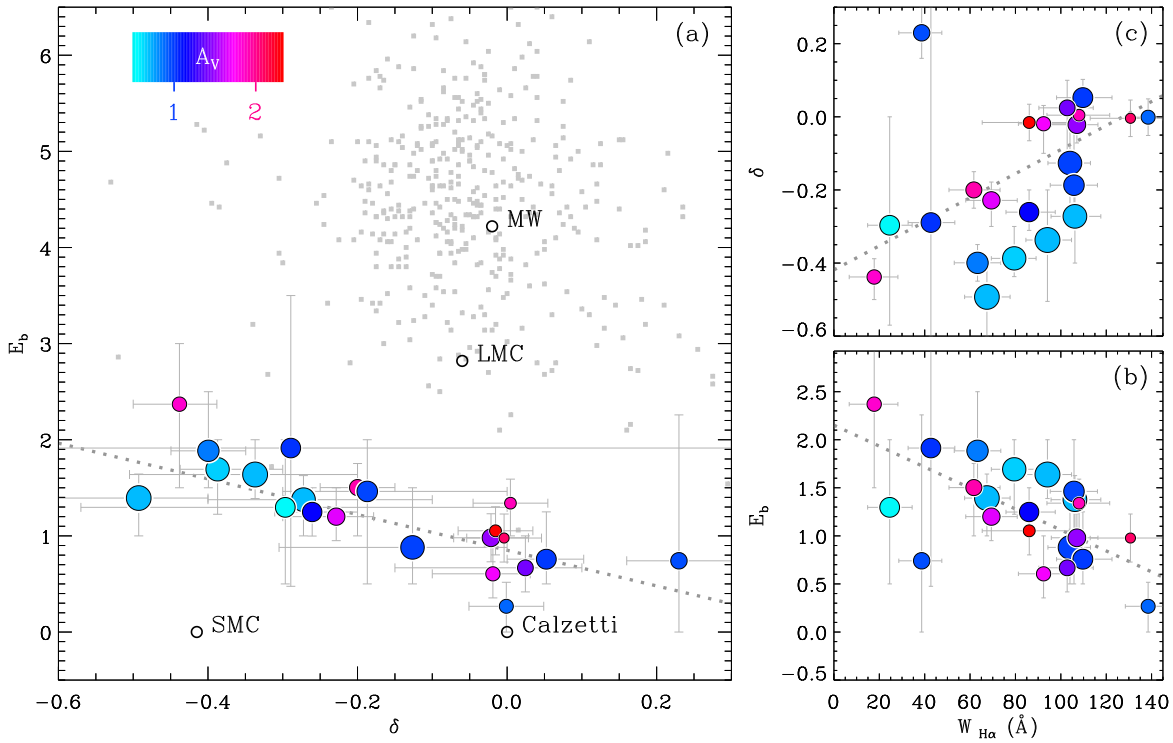

Figure 2. **a)** The best-fit values for the bump strength (E_B) and the slope (δ) of the dust attenuation curve for the different SED types. The size of the symbol reflects the number of galaxies used to construct the composite SED, and the color indicates the best-fit value for A_V (given the best-fit dust law). Galaxy types with $A_V < 0.5$ (which have primarily quiescent stellar populations) are not included in this figure, as the dust law could not be constrained well. There is a clear correlation between the slope of the attenuation curve and the UV bump strength. The Calzetti, MW, LMC and SMC attenuation and extinction curves are indicated by the open circles, and the small gray squares represent the MW sight-lines by Valencic et al. (2004). **b-c)** The bump strength and slope as a function of the total equivalent width of Hα. The dust attenuation is shallower and smoother in galaxies with higher $W_{\rm H\alpha}$ (i.e., higher specific SFRs).

also visible, among which Mg II, the Balmer and 4000 Å break, and the dust absorption feature at 2175 Å.

3. CONSTRAINING THE DUST ATTENUATION LAW

We constrain the dust attenuation curve by fitting the composite SEDs with the FSPS models in their default setting. These settings include a low contribution from thermally-pulsing asymptotic giant branch stars (e.g., Conroy & Gunn 2010; Kriek et al. 2010; Zibetti et al. 2013). We assume a Chabrier (2003) IMF and an exponentially declining star forming history (SFH), though our results are robust against the choice of IMF or parameterization of the SFH. We explore a grid of stellar ages, star formation timescales and three different metallicities (0.0096, 0.019 ($Z_\odot$), & 0.03). We use the stellar population fitting code FAST (Kriek et al. 2009), which is based on a simple χ^2 minimization. For the photometric uncertainties we assume a flat error in F_λ of 3% of the average flux, in order to ensure that the full SED shape will be taken into account in the fit. If we would use the formal errors, the fit would be driven completely by the very small error bars at longer wavelengths. The region around Hα is masked in the fit. The confidence intervals are calibrated using Monte Carlo simulations.

First, we explore both the MW and the Calzetti dust attenuation curves, and find the best-fit stellar population model when allowing all other parameters to vary. Next, we parameterize the dust attenuation curve following the prescription by Noll et al. (2009):

$$A(\lambda) = \frac{A_V}{4.05}(k'(\lambda) + D(\lambda)) \left(\frac{\lambda}{\lambda_V}\right)^{\delta} \quad (1)$$

with D the Lorentzian-like Drude profile to parameterize the UV bump, defined as:

$$D(\lambda) = \frac{E_b(\lambda\,\Delta\lambda)^2}{(\lambda^2 - \lambda_0^2)^2 + (\lambda\,\Delta\lambda)^2} \quad (2)$$

For the central wavelength of the dust feature λ_0 we adopt 2175 Å. $\Delta\lambda$ is the full width at the half maximum of the feature and we assume a value of 350 Å as found by Noll et al. (2009) from a stack of a spectra of high-redshift galaxies and by Seaton (1979) for the MW UV bump. We explore a grid of values for $E_{\rm b}$ and δ, while leaving all other fitting parameters free.

In Figure 1 we show the best-fit stellar population models for three composite SEDs, for the three different attenuation laws. This figure illustrates that for all three SEDs the Calzetti and MW law provide poor fits at rest-frame UV wavelengths. When leaving both the slope and bump strength as free parameters, we can reproduce their full SED shapes.

The best-fit values for $E_{\rm b}$ and δ for all composite SEDs with $A_V > 0.5$ are shown in Figure 2a. There is a clear correlation between both properties, described by the following linear fit:

$$E_b = (0.85 \pm 0.09) - (1.9 \pm 0.4)\,\delta \quad (3)$$

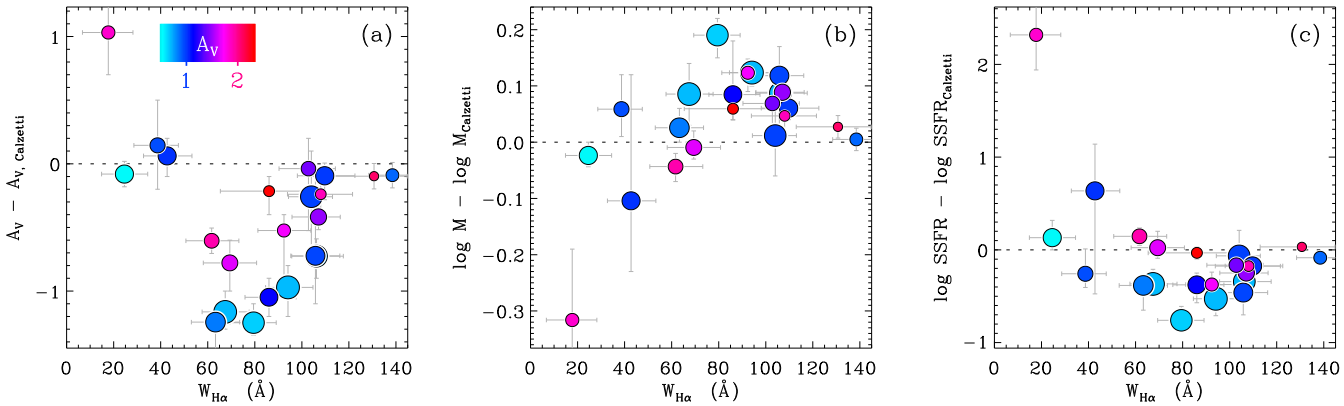

Figure 3. The difference in derived galaxy properties (A_V, stellar mass, specific SFR) between a free dust attenuation curve and the Calzetti law. The symbols are similar as in Figure 2. These panels illustrate that a universal dust law, implemented as a simple screen, may result in large systematic biases in derived galaxy properties.

SED types with steeper attenuation curves have stronger UV bumps, while shallower attenuation curves go together with weaker UV bumps.

4. CORRELATIONS WITH SPECTRAL TYPE

In the previous section we found a large variety in dust attenuation curves among the different SED types. In order to examine whether the shape of the dust law correlates with spectral type, we show both E_b and δ as a function of the equivalent width of Hα ($W_{H\alpha}$) in Figures 2b and c. Similar to the specific SFR, $W_{H\alpha}$ is a measure of the present to past star formation in a galaxy. This measurement directly follows out of the composite SEDs, and thus is independent of the SPS modeling. We do note that $W_{H\alpha}$ may include some contamination by [N II] and [S II], and thus may be slightly overestimated.

Figures 2b and c show that the shape of attenuation curve is correlated with spectral type. Star-forming galaxies with high values for $W_{H\alpha}$ have shallower attenuation curves with weaker UV bumps than galaxies with a quiescent star-forming mode. The only significant outlier to this trend is SED type 8, which is best fit by a shallow dust law ($\delta \sim 0.2$), while having a very low $W_{H\alpha}$. The least square fits give the following relations:

$$E_b = (2.2 \pm 0.3) - (1.1 \pm 0.3) \left(\frac{W_{H\alpha}}{100\text{Å}}\right) \quad (4)$$

$$\delta = (0.33 \pm 0.04) \left(\frac{W_{H\alpha}}{100\text{Å}}\right) - (0.41 \pm 0.04) \quad (5)$$

Our findings suggest that the dust attenuation curve should not be treated as a universal function, but should be related to the spectral type. In the next section we examine the implications of our results.

5. IMPLICATIONS

Comparing broadband SEDs or spectra with SPS models is a popular method to derive galaxy properties. In this procedure, the shape of the dust attenuation curve is almost always held fixed. Here we examine possible biases introduced by assuming the popular Calzetti dust attenuation law. Figure 3 shows the difference in best-fit galaxy properties for a free dust law compared to when assuming the Calzetti dust law. This figure illustrates that systematic biases may be introduced, when a universal dust law is assumed. A_V and the specific SFR may be significantly overestimated for galaxies with high $W_{H\alpha}$, while stellar mass may be slightly underestimated. For lower values of $W_{H\alpha}$ we may find the opposite effect. However, this effect is driven by only one SED type (12), which was already noticed in Kriek et al. (2011) as being poorly fit by any SPS model, and thus is not significant.

At high redshift dust attenuation corrections are frequently derived from the UV β slope ($F_\lambda \propto \lambda^\beta$), adopting the relation of Meurer er al. (1999). This relation was based on a UV slope measured by masking the UV bump and other features. In contrast, the measurements at high redshift are based on a small number of broadband filters (e.g., Reddy et al. 2010; Bouwens et al. 2012). In Figure 4 we use the composite SEDs to assess how the UV bump may influence the measurement of the UV slope, and hence the dust correction. In the top panel we show an example composite SED, the corresponding photometric measurements for two rest-frame UV filters for this SED, and the slopes based on the composite SED (dashed line) and photometric datapoints (dotted lines). In the lower panel we show the difference in the derived attenuation correction – based on the two UV slopes – versus the strength of the dust feature, for all composite SEDs with $A_V > 0.5$. This figure illustrates that the presence of a dust feature may lead to the underestimation of the dust correction, and thus the SFR. Stronger dust features clearly result in larger biases.

However, the illustration in Figure 4 is probably a worst case scenario, where only two filters are used, and the reddest filter completely overlaps with the UV bump. Several studies use three to four photometric bands (e.g., Bouwens et al. 2012) to measure the UV slope, resulting in more robust measurements. Furthermore, $W_{H\alpha}$ increases with increasing redshift (e.g., Stark et al. 2013), and thus at a redshift of $z = 6$ (used in the illustration in Fig. 4) or higher the bump may be insignificant. We do note though, that the utility of the UV slope for estimating dust attenuation has been called into question before (e.g., Kong et al. 2004; Johnson et al. 2007; Conroy et al. 2010b; Gonzalez-Perez et al. 2013).

6. DISCUSSION

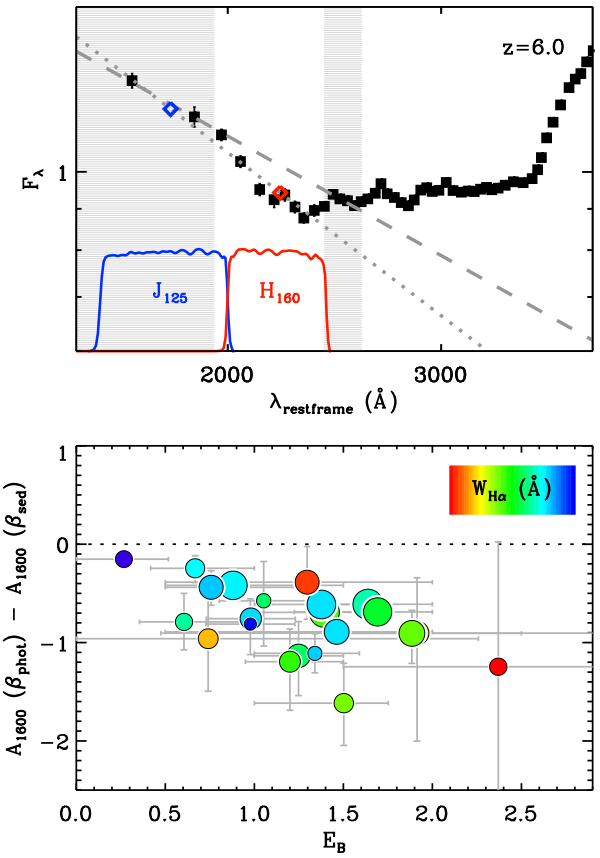

Figure 4. Implication for the dust correction based on the UV slope. The gray dashed line in the top panel represents the best-fit UV slope to the composite SED while masking the dust absorption feature. The datapoint sin the gray shaded area are included in the fit, following the prescription by Meurer er al. (1999). The gray dotted line shows the best-fit UV slope if we only had two photometric bands. In the lower panel we show the difference in derived values for A_{1600} using the relation by Meurer er al. (1999) versus the strength of the dust feature for all composite SEDs with $A_V > 0.5$. This figure illustrates that dust corrections based on photometric measurement, may be significantly underestimated, resulting in underestimated SFRs. However, the choice of filters in this illustration may possibly represent the worst case scenario, and different filters, redshifts, or the availability of multiple filters will lead to smaller biases.

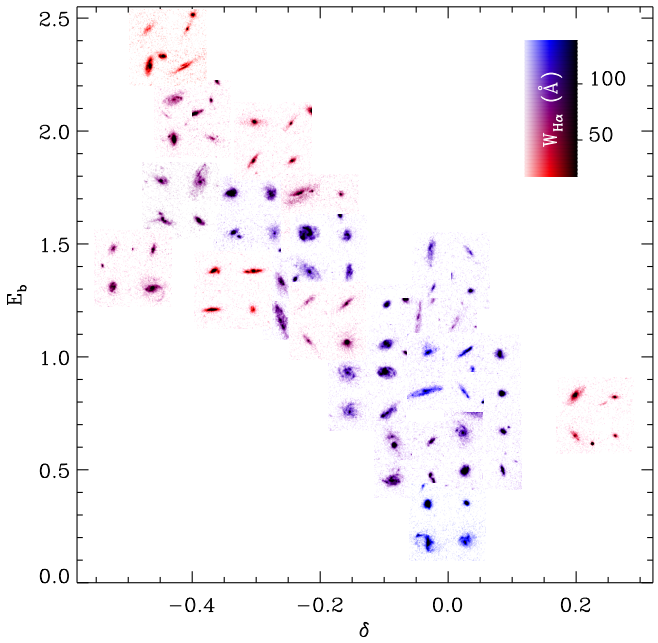

Figure 5. The bump strength (E_B) vs. the slope (δ) of the best-fit attenuation curve for all composite SEDs with $A_V > 0.5$ mag. Instead of symbols, we show the i-band HST images of 2-4 galaxies per SED type. The galaxies are chosen to be closest in redshift to $z = 0.9$, thus the images show the rest-frame optical morphologies. The images are color coded by the equivalent width of Hα (i.e, the specific SFR). This figure illustrates that galaxies with low $W_{H\alpha}$ and/or edge-on galaxies have steeper attenuation curves with stronger UV bumps, while face-on and/or high $W_{H\alpha}$ galaxies have shallower curves with weaker UV bumps.

The primary result of this Letter is that the shape of the dust attenuation curve varies with spectral type. This trend may be explained in part by a two-component dust model (e.g., Calzetti et al. 1994; Charlot & Fall 2000; Granato et al. 2000; Wild et al. 2011), in which all stars are attenuated by the diffuse ISM, while younger stars experience additional attenuation due to dust in their short-lived birth clouds. This model predicts that the shape of the attenuation curve should vary with specific SFR and galaxy inclination. In Figure 5, we plot E_b vs. δ, with HST morphologies instead of symbols (Scoville et al. 2007). This plot illustrates that face-on galaxies in general have shallower attenuation curves with weaker UV bumps. The slope is steepest and UV dust bump strongest for edge-on galaxies with low specific SFRs. Similar trends are also seen in local galaxies (Wild et al. 2011). Only SED type 8 (to the right of the diagram), which we mentioned before, does not seem to follow any of the trends.

The observed correlation between the attenuation curve and the specific SFR may also be due to variation in the UV radiation field (e.g., Gorden et al. 2003). In this picture, galaxies with high specific SFRs have harder UV radiation fields, which could destroy the grain population responsible for the UV bump. See Conroy (2013) for more discussion on the two proposed explanations for the observed trends.

Our values for E_b and δ are in the same range to those found by Buat et al. (2012), who fit the photometry of individual galaxies in the GOODS-S field. They also find weaker UV bump strengths in galaxies with larger specific SFRs (see also Wild et al. 2011). Buat et al. (2012) find no correlation though between the slope and the dust bump for their sample. This may not be surprising, as for individual galaxies the photometric resolution and S/N may not be sufficient to resolve the bump and to break modeling degeneracies. As a result the scatter in the measurements will be large, and possible trends may be washed out.

While the study presented in this Letter has been enabled by stacking SEDs of similar type, this is also a weakness, as we may be combining galaxies with different attenuation curves. Furthermore, the rest-frame wavelength coverage is not the same for all redshifts, and at bluer wavelengths the SEDs are dominated by the higher redshift galaxies in our sample. Thus, extending this study to shorter wavelengths, using GALEX data will give a more robust and representative measurement of the UV attenuation curve. Another drawback is that

we only look at the attenuated and not at the re-emitted light. In a future study we will extend the composite SEDs to longer wavelengths as well, so that we can simultaneously study the dust attenuation and emission as a function of spectral type.

7. SUMMARY

In this Letter, we use composite SEDs, constructed from NMBS photometry, to study variations in the dust attenuation curve in $0.5 < z < 2.0$ galaxies. Based on similarities between the full SED shapes, we have divided galaxies in different spectral classes and stacked the photometry. As each spectral type contains galaxies which span a range in redshift, the resulting SEDs are well sampled in wavelength and show various spectral features among which Hα and the 2175 Å dust feature.

We fit all composite SEDs by FSPS models, while exploring attenuation curves with varying slopes and UV bump strengths. The MW and Calzetti law provide poor fits at UV wavelengths for nearly all SED types. We find that the strength of the UV bump and the slope of the curve are strongly correlated, with steeper slopes having stronger UV dust bumps. Moreover, the shape of the dust attenuation curve correlates with the equivalent width of Hα (i.e., specific SFR), with higher $W_{\rm H\alpha}$ galaxies having shallower dust attenuation curves with weaker UV bumps. The average attenuation law has a UV bump strength of $\sim 25\%$ of the MW bump, and a slope in between the SMC and the MW extinction curve.

Our results are consistent with a two-component dust model, in which all stars are attenuated by the diffuse ISM, while young stars experience extra attenuation due to dust in their short-lived birth clouds. A qualitative analysis of the morphologies further supports this picture, as edge-on galaxies have on average steeper dust curves and stronger UV bumps. A varying grain size distribution, as a result of differences in the UV radiation field, may also be contributing to the observed correlations with Hα equivalent width.

A non-universal dust attenuation curve has numerous implications for galaxy evolution studies. By assuming a universal dust law, derived stellar population properties will suffer from systematic biases. For example, for the Calzetti law, the dust content and specific SFR may be significantly overestimated. Stellar mass measurements are more robust, and are only slightly underestimated. Furthermore, the biases vary with spectral type. The presence of the dust bump may also complicate dust corrections based the UV β slope. In the worst case scenario, when the reddest filter overlaps with the bump, A_{1600} could be underestimated by $\sim$1 mag, resulting in significantly underestimated SFRs. On a positive note, the observed variation should motivate theoretical work aimed at embedding self-consistent dust models into galaxy formation models.

We thank the members of the NMBS and COSMOS teams for the release of high-quality multi-wavelength data sets to the community. MK acknowledges support from HST grant HST-AR-12847.01-A. CC acknowledges support from the Alfred P. Sloan Foundation.

REFERENCES

Bouwens, R. J. et al. 2012, ApJ, 754, 83
Brammer, G. B., van Dokkum, P. G., & Coppi, P. 2008, ApJ, 686, 1503
Brammer, G. B., et al. 2011, ApJ, 739, 24
Buat, V., et al. 2011, A&A, 533, 93
Buat, V., et al. 2012, A&A, 545, 141
Burgarella, D., Buat, V., & Iglesias-Páramo, J. 2005, MNRAS, 360, 1413
Calzetti, D., Kinney, A. L., & Storchi-Bergmann T. 1994, ApJ, 429, 582
Calzetti, D., Armus, L., Bohlin, R. C., Kinney, A. L., Koornheef, J., & Storchi-Bergmann, T. 2000, ApJ, 533, 682
Chabrier, G. 2003, PASP, 115, 763
Charlot, S., & Fall, S., M. 2000, ApJ, 539, 718
Conroy, C., Gunn, J. E., & White, M. 2009, 699, 486
Conroy, C., & Gunn, J. E. 2010, ApJ, 712, 833
Conroy, C., Schiminovich, D., & Blanton, M. R. 2010b, ApJ, 718, 184
Conroy, C., White, M., & Gunn, J. E. 2010a, ApJ, 708, 58
Conroy, C. 2010, MNRAS, 404, 247
Conroy, C. 2013, ARAA, vol 51 (arXiv:1301.7095)
Draine, B. T. & Malhotra, S. 1993, ApJ, 414, 632
Elíasdottír, Á., et al. 2009, ApJ, 697, 1725
Gonzalez-Perez, V., Lacey, C. G., Baugh, C. M., Frenk, C. S., & Wilkins, S. M. 2013, MNRAS429, 1609
Gordon, K. D., Clayton, G. C., Misselt, K. A., Landolt, A. U., & Wolff, M. J. 2003, ApJ, 594, 279
Granato, G. L., Lacey, C. G., Silva, L., Bressan, A., Baugh, C. M., Cole, S., & Frenk, C. S. 2000, ApJ, 542, 710
Johnson, B. D., et al. 2007, ApJS, 173, 392
Kong, X., Charlot, S., Brinchmann, J., & Fall, S. M. 2004, MNRAS, 349, 769
Kriek, M., et al. 2009, ApJ, 700, 221
Kriek, M., et al. 2010, ApJ, 722, L64
Kriek, M., et al. 2011, ApJ, 743, 168
Labbé, I. et al. 2005, ApJ, 624, L81
Meurer, G. R., Heckman, T. M., & Calzetti D. 1999, ApJ, 521, 54
Noll, S., et al. 2009, A&A, 499, 69
Reddy, N. A., Erb, D. K., Pettini, M., Steidel, C. C., & Shapley, A. E. 2010, ApJ, 712, 1070
Scoville, N., et al. 2007, ApJS, 172, 1
Seaton, M. J. 1979, MNRAS, 187, 73
Stark, D. P., et al. 2013, ApJ, 763, 129
Stecher, T. P. 1965, ApJ, 142, 1683
Valencic, L. A., Clayton, G. C., & Gordon, K. D. 2004, ApJ, 616, 912
van Dokkum, P. G., et al. 2009, PASP, 121, 2
van Dokkum, P. G., et al. 2010, ApJ, 709, 1018
Whitaker, K. E., et al. 2010, ApJ, 719, 1715
Whitaker, K. E., et al. 2011, ApJ, 735, 86
Whitaker, K. E., et al. 2012, ApJ, 745, 179
Wild, V., Charlot, S. Brinchmann, J., Heckman, T., Vince, O., Pacifici, C., & Chevallard, J. 2011, MNRAS, 417, 1760
Witt, A. N., & Gordon, K. D. 2000, ApJ, 528, 799
Zibetti, S., Gallazzi, A., Charlot, S., Pierini, D. & Pasquali, A. 2013, MNRAS, 428, 1479